Strain relaxation and optical properties of etched $In_{0.19}Ga_{0.81}N$ nanorod arrays on the GaN template*

Zhang Dong-Yan(张东炎)[a)b)], Zheng Xin-He(郑新和)[a)†], Li Xue-Fei(李雪飞)[a)], Wu Yuan-Yuan(吴渊渊)[a)b)], Wang Hui(王 辉)[a)], Wang Jian-Feng(王建峰)[a)], and Yang Hui(杨 辉)[a)]

[a)] *Suzhou Institute of Nano-tech and Nano-bionics, Chinese Academy of Sciences, Suzhou* 215125, *China*
[b)] *Graduate University of the Chinese Academy of Sciences, Beijing* 100190, *China*

(Received 20 December 2011; revised manuscript received 9 February 2012)

InGaN/GaN epilayers, which are grown on sapphire substrates by the metal–organic chemical-vapour deposition (MOCVD) method, are formed into nanorod arrays using inductively coupled plasma etching via self-assembled Ni nanomasks. The formation of nanorod arrays eliminates the tilt of the InGaN (0002) crystallographic plane with respect to its GaN bulk layer. Photoluminescence results show an apparent S-shaped dependence on temperature. The light extraction efficiency and intensity of photoluminescence emission at low temperature of less than 30 K for the nanorod arrays are enhanced by the large surface area, which increases the quenching effect because of the high density of surface states for the temperature above 30 K. Additionally, a red-shift for the InGaN/GaN nanorod arrays is observed due to the strain relaxation, which is confirmed by reciprocal space mapping measurements.

Keywords: InGaN/GaN nanorod arrays, photoluminescence, strain relaxation, recombination

PACS: 78.66.Fd, 78.67.–n, 74.25.Gz **DOI:** 10.1088/1674-1056/21/8/087802

1. Introduction

Current high performance photovoltaic devices are exclusively based on the GaInP/(In)GaAs/InGaAs tandem solar cell with an efficiency higher than 42.1%.[1] Although significant progress has been achieved, improving the conversion efficiency is still the main task. A viable path to increase efficiency for solar cells is to adopt more junctions. Theoretical calculation has shown that in order to achieve photovoltaic efficiencies of greater than 50%, a sub-cell with band gap greater than 2.4 eV or 2.7 eV is required.[2] Such high band gaps are not readily available in other established material systems. Acting as a sub-cell, wide-band-gap InGaN alloys with an effective absorption and photo-current generation in a spectral range of 365 nm–460 nm can significantly enhance the conversion efficiency of light in this spectral range.

Due to p-type doping difficulty and crystal quality of In-rich InGaN alloys, most of the studies focused on p–i–n heterojunction solar cells with the Ga-rich intrinsic InGaN absorber.[3–8] Although InGaN materials have a high absorption coefficient up to 10^5 cm^{-1} at the band edge,[9] due to the critical thickness issue, there are still many challenges for the device design. To enhance photovoltaic (PV) action and increase light absorption which will significantly amplify the photocurrent generated from the i-region, p-GaN nanorod arrays were proposed.[10] Besides decreasing the loss of incident light, vertically oriented nanorod arrays with axial or coaxial structures can further provide the ability to accommodate the mismatch strain via lateral relaxation.[11] The use of InGaN/GaN p–n or p–i–n heterostructure nanorod arrays may be significant to realize group-III nitride solar cells.[12] Interestingly, (In)GaN nanorod arrays can be used as a template to regrow the InGaN layer (in axial configuration) with high quality due to dislocation- and strain-free characteristics.[13] However, some critical requirements or properties of GaN nanorod arrays as a template are still not reported yet. In this paper, an understanding of the mechanism of strain relaxation and optical properties of InGaN-based nanorod arrays is performed, which could result in a better prediction

*Project supported by the SONY-SINANO Joint Project (Grant No. Y1AAQ11001), the Suzhou Solar Cell Research Project, China (Grant No. ZXJ0903), and the International S & T Cooperation Projects (SINO-Japan), the Science Fund of the Ministry of Science and Technology of the People's Republic of China (Grant No. 2010DFA22770).

†Corresponding author. E-mail: xhzheng2009@sinano.ac.cn

© 2012 Chinese Physical Society and IOP Publishing Ltd

and design of heteroepitaxial growth behaviours for InGaN layers on the GaN nanorod array template.

In our study, $In_{0.19}Ga_{0.81}N$/GaN heterostruture nanorod arrays are fabricated, and their optical properties are investigated. The degree of relaxation for the as-grown sample and nanorod arrays are determined by the reciprocal space mapping (RSM) results. From PL measurements for InGaN/GaN nanorod arrays and films, we find that vertically-aligned InGaN/GaN nanorod arrays can emit about 1.5 times stronger than that of InGaN film at 10 K. Furthermore, a red-shift of the PL spectral peak position is observed in InGaN/GaN nanorod arrays. From the value of the red-shift, the pressure coefficient for the built-in biaxial strain in the InGaN layer at 10 K is calculated. At the same time, another sample with solely-formed nanorod arrays of the InGaN layer is fabricated for comparison.

2. Experiments

MOCVD-grown $In_{0.19}Ga_{0.81}N$/GaN epilayers were used to form nanorod arrays. The intrinsic InGaN layer has a thickness of 120 nm. The vertically-oriented nanorod arrays were prepared by inductively coupled plasma (ICP) etching of the InGaN or InGaN/GaN film with self-assembled Ni clusters as the etching mask.[14] The morphology and size distribution of InGaN/GaN nanorod arrays were estimated by field-emission scanning electron microscopy (FE-SEM). The FE-SEM images of the side-view are in Fig. 1(a). The total length of nanorods is about 1 μm, including 120-nm long InGaN and 880-nm long GaN nanostructures. The diameter and density of the nanorods is 100 nm–200 nm and 1.5×10^9 cm^{-2}, respectively. The layer structure of the InGaN/GaN-heterostruture nanorod arrays is shown in the inset of Fig. 1(a).

The X-ray diffraction (XRD) and RSM measurement were performed using a D8/Bruker DISCOVER high-resolution X-ray diffractometer, equipped with a four-crystal monochromator in Ge (220) and Ge (440) configuration and four-circle translational capability. The photoluminescence (PL) was excited by a 325-nm line of He–Cd laser with an excitation power of 20 mW. For low temperature measurements, samples were fixed on a cold finger of a closed-circuit helium cryostat.

3. Results and discussion

Figure 1(b) depicts the distribution of the scattered X-ray intensity in reciprocal space of the asymmetric (11-24) Bragg reflexes, which provides an effective tool for determining the strain states in InGaN/GaN heterostructures. Based on the ψ marked in the figure, the degree of relaxation for InGaN nanostructured arrays on GaN templates is about 100%. This is generally correct on the assumption that the lattice of thick GaN film is equal to that of bulk GaN crystal, and the 120-nm thick InGaN layer is not thick enough to change the lattice of the GaN layer underneath. So the illustration describes the strain relaxation process in the InGaN layer as the nanorod arrays are formed. The large aspect ratio of the nanorod permits strain relief in three dimensions as a result of the extra-free surface. GaN nanorod arrays provide a useful means for controlling and manipulating strain in InGaN layers, and the strain-relaxed growth can suppress the tendency toward phase separation in InGaN layers with high indium content.[15]

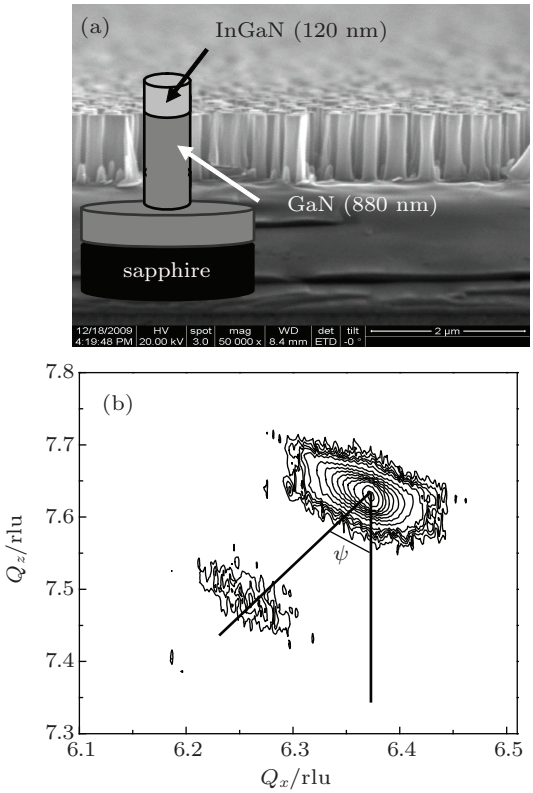


Fig. 1. (a) FE-SEM images of side view for InGaN/GaN nanorod arrays, the inset of panel (a) shows the layer structure, (b) RSM measured in the vicinity of (11-24) reflection.

To identify the effect of formed nanorod arrays of the GaN layer underneath on the degree of relaxation

and understand further the mechanism of relaxation in the InGaN nanorod arrays, the solely-formed nanorod arrays of the InGaN layer were fabricated and labelled as sample C. The depth of ICP etching in sample C is changed to be around 120 nm, which is equal to the thickness of the InGaN layer. To better distinguish the samples used in this paper, the sample aforementioned and the as-grown sample are labelled as sample A and sample B, respectively. Figure 2 shows the RSMs of asymmetric (11-24) Bragg reflexes of sample B and sample C. Although the thickness of the InGaN layer in sample B is about 20 times more than the "critical thickness", the in-plane lattice parameter is closely equal to the GaN lattice spacing, indicating that the InGaN layer of this heterostructure is fully strained. This is further evidence for the negligible relaxation in the InGaN layer with a thickness much more than the "critical thickness", which was calculated from the Mathews and Blakeslee model and the Fischer model.[11] In sample C, this situation is significantly changed. The degree of relaxation calculated from the RSM measurement is about 92.4%. We argue that the contact area between an InGaN rod and the GaN layer underneath is almost the same in sample A and sample C. Due to the same ratio of the large InGaN nanorod surface area in comparison to its volume and the contact area, it is found that the InGaN layers in sample A and sample C have almost the same degrees of relaxation. From this, we believe that the assumption that the lattice of thick GaN film equals that of bulk GaN crystal is valid. On the other hand, some reports showed theoretically that nanorod strain at the heterointerface decreases rapidly within a few atomic layers, and then fully relaxes in several manometers.[16,17] The results of fully relaxed InGaN layers in the two samples showed experimentally that a nanorod has a great ability to accommodate the mismatch in the overlayer, even though the underlayer is still in the planar structure.

Additionally, according to the measured relaxation, In content in the InGaN layer is easily calculated via fitting to the experiment data of $\omega/2\theta$ scan (not shown here). Using the Vegard's law, the In composition in our sample was estimated to be about 0.19. Meanwhile, a dependence of diffracted angle on the sample rotation normal to the surface indicates that the InGaN (0002) crystallographic plane has an angular offset from the (0002) crystallographic plane of the GaN layer underneath in sample B, and the tilt is about 0.01° along the (10-10) direction. However, the tilt of the InGaN (0002) crystallographic plane is eliminated in sample A and sample C, which could be attributed to the strain relaxation.

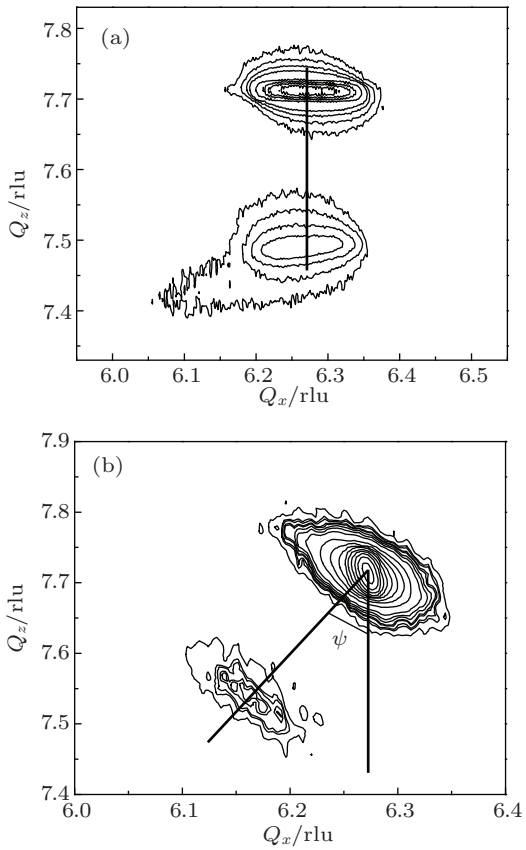


Fig. 2. RSMs measured in the vicinity of (11-24) reflection for samples B (a) and C (b).

These changes in structural properties are further characterized by PL. Figure 3 shows the PL responses for sample A and sample B at a temperature range from 7 K to 80 K, and the PL spectrum of sample C is not shown here due to its similar behaviour to that of sample A. The PL peaks for the three samples show an apparent S-shaped dependence on the temperature.[18] The PL intensity of InGaN/GaN nanorod arrays is about 1.5 times stronger than that of sample B at 10 K. The emission enhancement could result from the improvement in external quantum efficiency because of the low effective index and reduced loss from reflection of incident light, which has been reported elsewhere.[10] Due to the sidewall of the nanorod, the larger possibility for photons to escape could also contribute to the increase in light emission from our InGaN/GaN nanorod arrays.

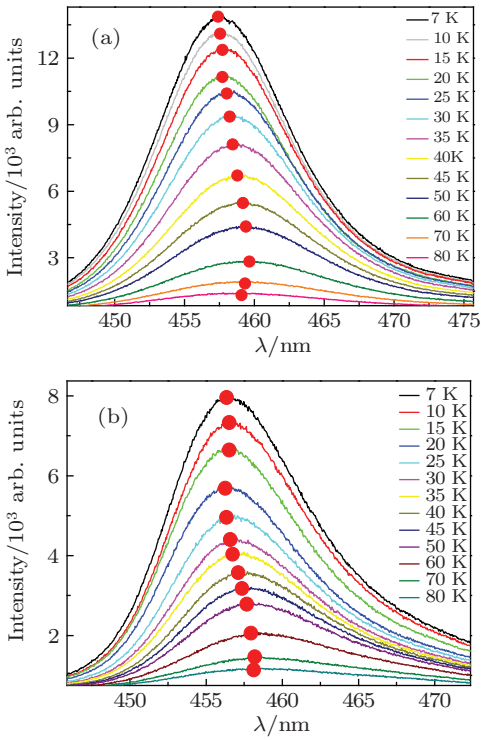


Fig. 3. (colour online) PL spectra at temperatures ranging from 7 K to 80 K for sample A (a) and sample B (b).

The temperature-dependence PL properties for sample A and sample B were studied at temperatures between 7 K and 200 K in Fig. 4(a). Note that a shift of the emission peaks to a longer wavelength for the InGaN/GaN nanorod arrays in comparison to sample B can be observed due to strain relaxation, which is the only difference in the InGaN layer between sample A and sample B. As is well known, the band gap of InGaN can be changed by the atom size effect or lattice constant, which is affected by the application of hydrostatic pressure.[19] The light emission energy peak would shift toward a shorter wavelength when the hydrostatic pressure increases. Actually, the built-in biaxial stress in the InGaN layer can act as a hydrostatic pressure to modify the pressure behaviour of InGaN.[20,21] So, it is supposed that the red-shift is reversed when the built-in biaxial strain is relaxed. From the red-shift value of 5.7 meV for the nanorod arrays, the pressure coefficient for the built-in biaxial stress in the InGaN layer is about 2 meV/GPa–8 meV/Gpa under 10 K (the in-plane biaxial stress in the InGaN layer can be obtained from the relationship: $\sigma = Gf$,[22] where G is the shear modulus,[23] f is the in-plane strain component expressed as $f = (a - a_0)/a_0$, with a and a_0 being the strained and fully relaxed lattice parameters, respectively). The biaxial stress would lead to an increase of $\sim 20\%$ in the pressure coefficient for InGaN alloys, which is in a range from 20 meV/GPa to 40 meV/Gpa.[19] For an InGaN film with In content of 0.19, if the degree of relaxation is equal to 100%, the thickness must be up to 800 nm or more.[24,25] There have been few reports to analyse quantitatively the effects of the built-in biaxial strain on the pressure coefficient. In bulk InGaN-based top cells, different degrees of relaxation affected by the thickness of the absorber would result in the shift of absorption, which should be designed carefully in multi-junction solar cells. The strain-free InGaN absorber grown on the GaN nanorod arrays allows the precise control of the absorption as the top cell to better match the incident solar spectrum.

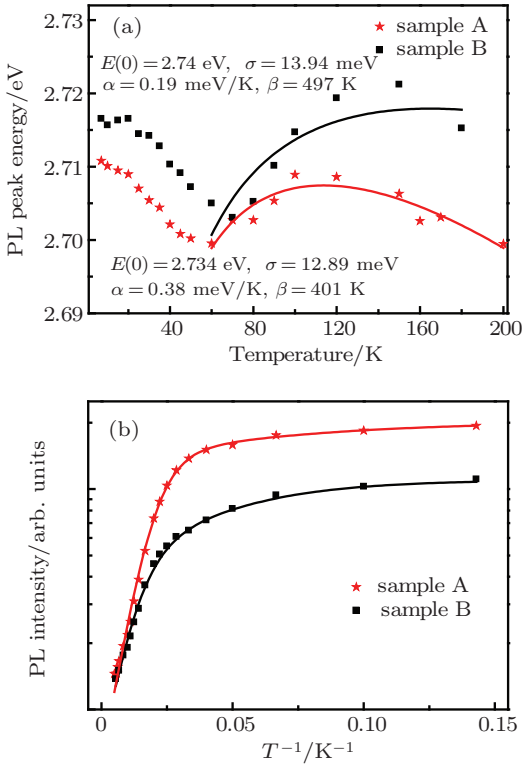


Fig. 4. (colour online) Dependences of PL peaks on T (a) and $1/T$ (b) for sample A and sample B, where the solid lines denote the fitted curves to Eq. (1) (a), the Arrhenius plots of integrated PL intensity for the sample A and sample B (b).

In Fig. 4(a), the fit was used to obtain the peak position dependence on temperature via the band-tail model[26,27]

$$E(T) = E(0) - \frac{\alpha T^2}{T + \beta} - \frac{\sigma^2}{k_{\mathrm{B}} T}, \qquad (1)$$

where $E(0)$ is the energy band gap at zero temperature, α and β are Varshni's fitting thermal coefficients. The last term on the right-hand side comes from the

localization effect, and σ is the characteristic parameter describing the shape of the energy band-tail, and $k_{\rm B}$ is Boltzmann's constant. The fitting parameters of $\sigma = 12.89$ meV and 13.94 meV for the sample A and sample B are of the same order as the reported values for quantum well (QW) systems ($\sim$ 30 meV).[28] This implies that the structure of nanorod arrays affects the PL behaviour due to the strain relaxation, but does not influence the localization effect resulting from the indium composition fluctuation.

Figure 4(b) shows an Arrhenius plot of the integrated PL intensity for sample A and sample B from 7 K to 200 K. Thermal quenching of the integrated PL intensity due to activation of nonradiative channels can be observed for temperatures higher than 30 K. As the temperature increases, the integrated PL intensities decrease by a factor of 11.2 and 6.5 for sample A and sample B, respectively. The results imply that the thermal quenching of the luminescence behaviour of nanorod arrays in sample A is worse than that of sample B. Considering two different recombination centres, the activation energy in a thermally activated process can be calculated by the following expression:[29,30]

$$I(T) \propto \frac{1}{1 + \sum\limits_{i=1} S_i \exp\left(-\dfrac{E_i}{k_{\rm B}T}\right)}, \qquad (2)$$

where E_i are the activation energies of the corresponding nonradiative recombination centres, S_i are rate constants related to the density of these centres, and $k_{\rm B}$ is Boltzmann's constant. A good fit to our experimental data (solid line) is obtained if two nonradiative channels are included, and the results are presented in Table 1. It is found that the value of activation energy E_2 ($\sim$ 14 meV) of the two samples changes little, implying that the origins of the nonradiative recombination centres at high temperatures are the same because of their similar activation energies. The activation energies are not only much smaller than the QW binding energy of the excitons, but also smaller than the energies of nonradiative centres related to dislocations.[31] Additionally, a larger rate constant of 34.33 is observed for the nanorod arrays. This may result primarily from the morphology of the nanoscale structure, and more defects induced by the ICP etching. Actually, the total surface area of the InGaN layer for nanorod arrays is about 1.5 times that for sample B. Therefore, we conclude that high density of surface state is one of the major factors for a large value of S_2 and thus a terrible quenching effect in nanorod arrays. So it is necessary to use some post-processes (such as thermal annealing, chemical method or oxidation process) to heal the surface state caused by the ICP etching. The experiments are under way. It is interesting to note that at low temperature radiative recombination is a dominant process. The activation energies for both samples are very close to $k_{\rm B}T$ when T is 30 K ($\sim$ 2.7 meV), and the rate constant is very small. So this nonradiative centre can be explained by the escaping of carriers captured at the localized potential minima or thermal quenching of bound excitons.[32] However, the real origin of this nonradiative channel and the type of bound exciton in this process are not known. It could be supposed that the much lower rate constants (in Table 1) for sample A and sample C are attributed to the strain relaxation because of the formation of nanorod arrays. This implies that carriers could have better opportunity to be confined into localization states before nonradiative recombination at lower temperature.

Table 1. Fitted results with respect to the experimental temperature-dependent PL integrated intensities for the three samples.

Samples	S_1	E_1/meV	S_2	E_2/meV
A	0.60	1.72	34.33	14.01
B	1.77	2.80	14.84	13.84
C	0.27	1.84	18.7	13.36

4. Conclusion

In this paper, the InGaN/GaN film is fabricated into nanorod arrays. The RSM results show that the formation of nanorod arrays leads to an almost full relaxation compared with the case of the as-grown sample. From the complete relaxation, the pressure coefficient is calculated to be 2 meV/GPa–8 meV/Gpa under 10 K for the built-in biaxial strain in the InGaN layer. The formation of nanorod arrays increases the nonradiative recombination due to more surface states at high temperature, but increases radiative recombination at a lower temperature.

References

[1] Takamoto T, Kaneiwa M, Imaizumi M and Yamaguchi M 2005 *Prog. Photovoltaics* **13** 495

[2] Barnett A, Kirkpatrick D, Honsberg C, Moore D, Wanlass M, Emery K, Schwartz R, Carlson D, Bowden S, Aiken D, Gray A, Kurtz S, Kazmerski L and Moriarty T 2007 *The 22nd European Photovoltaic Solar Energy Conference*
[3] Jani O, Ferguson I, Honsberg C and Kurtz S 2007 *Appl. Phys. Lett.* **91** 132117
[4] Zheng X H, Horng R H, Wuu D S, Chu M T, Liao W Y, Wu M H, Lin R M and Lu Y C 2008 *Appl. Phys. Lett.* **93** 261108
[5] Chen X, Matthews K D, Hao D, Schaff W J and Eastman L F 2008 *Phys. Status Solidi* A **205** 1103
[6] Neufeld J, Toledo N G, Cruz S C, Iza M, DenBaars S P and Mishra U K 2008 *Appl. Phys. Lett.* **93** 143502
[7] Horng R H, Lin S T, Tsai Y L, Chu M T, Liao W Y, Wu M H, Lin R M and Lu Y C 2009 *IEEE Electron Dev. Lett.* **30** 724
[8] Zhang X B, Wang X L, Xiao H L, Yang C B, Hou Q F, Yin H B, Chen H and Wang Z G 2011 *Chin. Phys.* B **20** 028402
[9] Muth J F, Lee J H, Shmagin I K, Kolbas R M, Casey H C, Keller B P, Mishra U K and DenBaars S P 1997 *Appl. Phys. Lett.* **71** 2572
[10] Zhang D Y, Zheng X H, Tang L J, Dong J R, Wang H and Yang H 2010 *IEEE Electron Dev. Lett.* **31** 1422
[11] Ertekin E, Greaney P A, Chrzan D C and Sands T D 2005 *J. Appl. Phys.* **97** 114325
[12] Seo H W, Tu L W, Lin Y T, Ho C Y, Chen Q Y, Yuan L, Norman D P and Ho N J 2009 *Appl. Phys. Lett.* **94** 201907
[13] Ye H, Lu P F, Yu Z Y, Song Y X, Wang D L and Wang S M 2009 *Nano Lett.* **9** 1921
[14] Chiu H, Lo M H, Lu T C, Yu P C, Huang H W, Kuo H C and Wang S C 2008 *J. Lightwave Technol.* **26** 1445
[15] Kuykendall T, Ulrich P, Aloni S and Yang P 2007 *Nat. Mater.* **6** 951
[16] Zervos M and Feiner L F 2004 *J. Appl. Phys.* **95** 281
[17] Swadener J G and Picraux S T 2009 *J. Appl. Phys.* **105** 044310
[18] Xu G Z, Liang H, Bai Y Q, Lau K M and Zhu X 2005 *Acta Phys. Sin.* **54** 5344 (in Chinese)
[19] Wu J Q 2009 *J. Appl. Phys.* **106** 1
[20] Suski T, Teisseyre H, Lepkowski S P, Perlin P, Mariette H, Kitamura T, Ishida Y, Okumura H and Chichibu S F 2003 *Phys. Status. Solidi* B **235** 225
[21] Shan W, Walukiewicz W, Haller E E, Little B D, Song J J, McCluskey M D, Johnson N M, Feng Z C, Schurman M and Stall R A 1998 *J. Appl. Phys.* **84** 4452
[22] Harutyunyan V S, Aivazyan A P, Weber E R, Kim Y, Park Y and Subramanya S G 2001 *J. Phys.* D: *Appl. Phys.* **34** A35
[23] Jian S R, Fang T H and Chuu D S 2006 *Appl. Surf. Sci.* **252** 3033
[24] Faleev N, Jampana B, Jani O, Yu H B, Opila R, Ferguson I and Honsberg C 2009 *Appl. Phys. Lett.* **95** 051915
[25] Guo X, Wang H, Jiang D S, Wang Y T, Zhao D G, Zhu J J, Liu Z S, Zhang S M and Yang H 2010 *Chin. Phys.* B **19** 106802
[26] Zheng X H, Chen H, Yan Z B, Li D S, Yu H B, Huang Q and Zhou J M 2004 *J. Appl. Phys.* **96** 1899
[27] Eliseev P G, Perlin P, Lee J Y and Osinski M 1997 *Appl. Phys. Lett.* **71** 569
[28] Cho Y H, Gainer G H, Fischer A J, Song J J, Keller S, Mishra U K and DenBaars S P 1998 *Appl. Phys. Lett.* **73** 1370
[29] Bimberg D, Sonderge M and Grobe E 1971 *Phys. Rev.* B **4** 3451
[30] Lai Y L, Liu C P, Lin Y H, Lin R M, Lyu D Y, Peng Z X and Lin T Y 2006 *Appl. Phys. Lett.* **89** 151906
[31] Hao M, Zhang J, Zhang X H and Chua S 2002 *Appl. Phys. Lett.* **81** 5129
[32] Yasan A, McClintock R, Mayes K, Kim D H, Kung P and Razeghi M 2003 *Appl. Phys. Lett.* **83** 4083